

---

# Dual Data Alignment Makes AI-Generated Image Detector Easier Generalizable

---

Ruoxin Chen<sup>1</sup>, Junwei Xi<sup>2</sup>, Zhiyuan Yan<sup>3</sup>, Keyue Zhang<sup>1</sup>, Shuang Wu<sup>1</sup>,  
Jingyi Xie<sup>4</sup>, Xu Chen<sup>2</sup>, Lei Xu<sup>5</sup>, Isabel Guan<sup>6†</sup>, Taiping Yao<sup>1†</sup>, Shouhong Ding<sup>1</sup>

<sup>1</sup>Tencent YouTu Lab, <sup>2</sup>East China University of Science and Technology,

<sup>3</sup>Peking University, <sup>4</sup>Renmin University of China,

<sup>5</sup>Shenzhen University, <sup>6</sup>Hong Kong University of Science and Technology

† Corresponding Authors

{cusmochen, taipingyao}@tencent.com, eeguan@ust.hk

## Abstract

The rapid increase in AI-generated images (AIGIs) underscores the need for detection methods. Existing detectors are often trained on biased datasets, leading to overfitting on spurious correlations between non-causal image attributes and real/synthetic labels. While these biased features enhance performance on the training data, they result in substantial performance degradation when tested on unbiased datasets. A common solution is to perform data alignment through generative reconstruction, matching the content between real and synthetic images. However, we find that pixel-level alignment alone is inadequate, as the reconstructed images still suffer from frequency-level misalignment, perpetuating spurious correlations. To illustrate, we observe that reconstruction models restore the high-frequency details lost in real images, inadvertently creating a frequency-level misalignment, where synthetic images appear to have richer high-frequency content than real ones. This misalignment leads to models associating high-frequency features with synthetic labels, further reinforcing biased cues. To resolve this, we propose Dual Data Alignment (DDA), which aligns both the pixel and frequency domains. DDA generates synthetic images that closely resemble real ones by fusing real and synthetic image pairs in both domains, enhancing the detector’s ability to identify forgeries without relying on biased features. Moreover, we introduce two new test sets: DDA-COCO, containing DDA-aligned synthetic images, and EvalGEN, featuring the latest generative models. Our extensive evaluations demonstrate that a detector trained exclusively on DDA-aligned MSCOCO improves across diverse benchmarks. Code is available at <https://github.com/roy-ch/Dual-Data-Alignment>.

## 1 Introduction

The rise of AIGIs [12, 18, 41, 49] poses risks to digital security, including the potential for misinformation, fraud, and copyright violations [12, 20, 21, 18, 34, 54, 52, 51, 47, 24, 36]. This severe security issue underscores the urgent need for reliable detection methods to differentiate synthetic images from authentic ones. Despite advances in AIGI detection techniques [4, 32, 35], the rapid evolution of generative models and the emergence of new architectures present cross-domain generalization challenges. This is especially evident in zero-shot scenarios involving previously unseen generation paradigms.

The generalizability of AIGI detectors is hindered by dataset biases [13, 4, 33, 14]. Existing datasets often exhibit systematic discrepancies in attributes unrelated to the authority. Works [38] illustrate semantic bias through word frequency analysis, and studies [35] demonstrate image size bias by

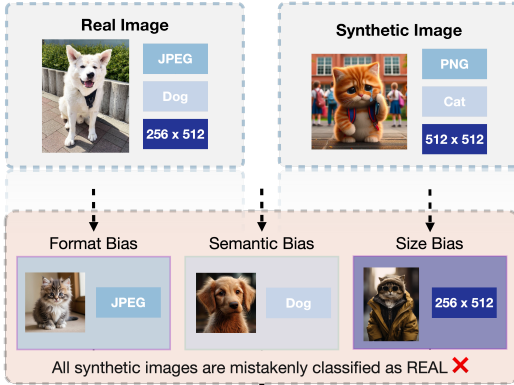


Figure 1: **Illustration of dataset bias.** Top row: Real/synthetic images show disparities in format, content, and size. Real images are typically in JPEG, with varying sizes and centered semantics. Bottom row: Detectors trained on datasets containing these discrepancies are prone to learning biased features, incorrectly associating authenticity with format, image size, or semantics.

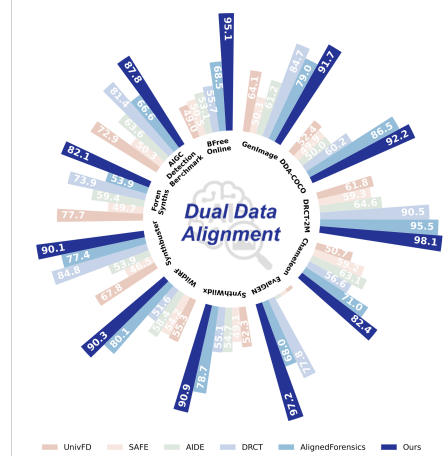


Figure 2: **Overall comparison between detection methods on 11 benchmarks.** Our model is exclusively trained on DDA-aligned MSCOCO data. The consistent outperformance of DDA on 4 in-the-wild (Chameleon, WildRF, BFree-Online and SynthWildx) and 7 manually-crafted benchmarks validates the generalizability. Detailed results are provided in Section 4.

analyzing on the datasets where synthetic images are uniformly sized as multiples of  $128 \times 128$ . These non-causal features could be exploited by models to distinguish real from synthetic images, resulting in biased detector performance that fails to generalize across different datasets. Figure 1 visually illustrates such bias. **Dataset alignment holds promise in addressing the issue of dataset bias** by ensuring synthetic images closely resemble real ones, *excluding authenticity-related factors and directing detectors to focus on forgery-related cues*. Specifically, studies [13] reveal systematic discrepancies in format and size biases: real images are JPEG-encoded and vary in size, whereas synthetic images are uniformly PNG-encoded and fixed in size. SemGIR [53], DRCT [4], B-Free [14] aim to mitigate content discrepancies using diffusion reconstruction techniques that generate images semantically similar to real ones. Works [15, 55, 58] prevent models from learning semantics-dependent features by breaking images into patches and shuffling them.

However, in this paper, we ask: *Does reconstruction truly eliminate potential misalignment and bias?* Our answer is **no**. We find that although reconstruction-based methods align datasets at the pixel level, they still **introduce subtle misalignments at the frequency level**. Specifically, generative reconstruction based data alignment tends to preserve or even amplify details across all frequency bands. In particular, reconstructed images often restore high-frequency components that are diminished in real images—typically due to compression during transmission or storage, where such components are removed to reduce file size because they have little impact on human visual perception. Consequently, **synthetic images exhibit disproportionately strong high-frequency details, whereas real images contain much weaker ones**, creating a noticeable discrepancy in the magnitude of high-frequency components rather than in their semantic content. This spurious correlation can lead detectors to overfit these frequency cues, mistakenly identifying high-frequency richness as an indicator of synthetic origin.

In this paper, we propose **Dual Data Alignment (DDA)**, an effective technique that aligns synthetic images with real ones across both pixel and frequency domains. DDA consists of three steps: 1) VAE reconstruction for pixel alignment, 2) high-frequency fusion to eliminate bias, and 3) pixel mixup for further alignment in the pixel domain. As shown in Figure 2, **a single model trained on DDA-aligned MSCOCO demonstrates significant improvements across benchmarks: +11.4% on Chameleon, +26.6% on BFree-Online and +19.4% on EvalGEN, with much lower fluctuations across subsets – usually 1/2 that of baselines.** We attribute this significant performance boost to the data alignment process: when synthetic images are carefully aligned with real images across key domains, the model learns a tighter, more transferable decision boundary, enhancing generalizability

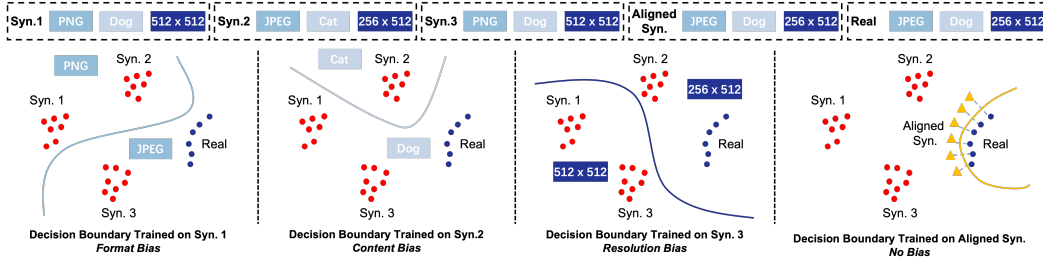


Figure 3: Visual illustration of how dataset bias affects decision boundaries. **Left three panels:** Detectors trained on biased data—where synthetic images (e.g., Syn.1–3) differ from real images in format, content, or resolution—tend to learn spurious decision boundaries. **Right:** When synthetic images are carefully aligned with real images across multiple aspects, the model can learn a tighter decision boundary that more accurately encompasses the real data.

to unseen data, as demonstrated in Figure 3. Moreover, we introduce two new evaluation datasets: 1) DDA-COCO, a test set consisting of real images from MSCOCO and their DDA-aligned counterparts. This dataset evaluates whether the detector captures inherent discriminative features or relies on other biases. Prior detectors suffer significant performance drops on DDA-COCO. 2) EvalGEN, a test set consisting of FLUX, GoT, Infinity, NOVA, and OmniGen, which includes both advanced auto-regressive and diffusion generators, serving for measuring detectors’ generalizability under newly evolved generative models.

## 2 Related Works

**AIGI Detection.** CNNSpot [42] trains a vanilla CNN model, finding that detectors easily recognize synthetic images from seen models but struggle to generalize to unseen ones. UnivFD [32] employs CLIP as backbone, showing the improvements in generalizability in detecting unseen generators. Subsequent works [25, 38, 55, 50] explore model architectures and image preprocessing for more generalizable detection. C2P-CLIP enhances the pretrained CLIP backbone for AIGI detection by injecting ‘real’ and ‘fake’ concepts. Works [39, 6, 23, 19, 57] exploit frequency domain artifacts, showing that frequency artifacts could well discriminate. NPR [40] explores the upsampling artifact in generative models. Vision–language approaches [27, 17, 26, 5, 46, 45] pursue explainable detection by leveraging VLMs’ semantic priors. However, these methods’ generalizability is limited by either content bias or frequency-level bias, with a chance of exploiting non-causal features like image format, which can degrade performance on unbiased test sets.

**Dataset alignment.** The evaluation bias issue in AIGI detection is firstly introduced in the work [13], showing that image format and size are common biases unintentionally exploited by detectors. FakeInversion [3] introduces a bias-reduced evaluation benchmark, mitigating thematic and stylistic biases by collecting synthetic images that match real images in both content and style. A line of subsequent works explores eliminating bias in the training set to enhance generalizability. SemGIR [53] regenerates synthetic images by semantic-level reconstruction conditioned on the real counterpart’s description, aiming to better align synthetic and real images semantically. DRCT [4] employs diffusion reconstruction for improved semantic alignment. B-Free [14] addresses dataset bias through self-conditioned inpainted reconstructions and content augmentation. However, this inpainting paradigm can alter the center object, corrupting the semantic alignment. AlignedForensics [33] performs simple VAE reconstruction without latent space manipulation, resulting in synthetic images that closely match real images in semantics and resolution. However, both B-Free and AlignedForensics overlook format alignment, creating space for JPEG-based shortcuts in discrimination.

## 3 Methodology

### 3.1 Motivation and Analysis

**Misaligned Dataset.** In the absence of additional supervision, detectors rely exclusively on the training set to learn the concept of ‘real’ versus ‘synthetic’. When these two classes’ data differ systematically in non-causal attributes—such as compression format or semantic content—the model may incorrectly learn to associate these irrelevant features with authenticity. These spurious signals

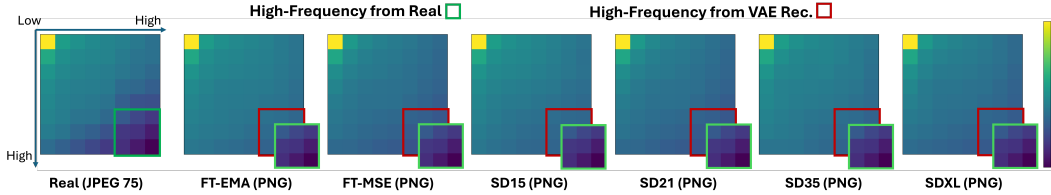


Figure 4: **Visualization of frequency domain energy using 2D DCT.** The left column shows a real image, while the remaining columns display images reconstructed by VAEs from various Stable Diffusion models. The grids represent frequency components, with the top-left and bottom-right indicating low- and high-frequency regions, respectively. Lighter areas correspond to higher energy. Real images in JPEG format exhibit darker high-frequency regions compared to VAE reconstructions, indicating weaker high-frequency content in real images.

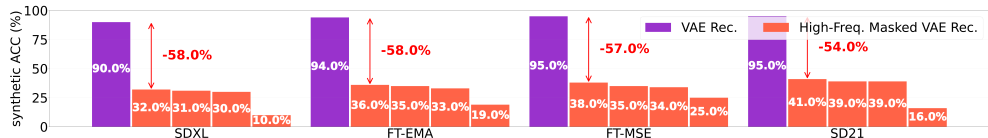


Figure 5: **Evidence for the existence of biased frequency-based features to discriminate reconstructed images.** We apply a binary mask to the DCT coefficients, systematically nullifying high-frequency components where either the horizontal or vertical frequencies exceed 95%, 90%, 85% and 80% of their respective spectral ranges to generate High-Freq. Masked VAE Rec.

are often more salient than subtle, genuine artifacts that actually distinguish real from synthetic images, making it more difficult for the model to learn truly generalizable features.

**Reconstruction-based Alignment.** To align synthetic images with real ones, some approaches [53, 59, 14] employ txt2img generative models to generate images with similar semantic content, conditioned on the image label or image captions obtained through pretrained models. However, images generated using this approach often differ from the originals due to the lack of strong and detailed supervision, which prevents the generated images from fully matching the original images in all semantic details. DRCT [4, 14] leverages Img2Img diffusion reconstruction, directly using the image itself to guide the reconstruction of a real image  $x$  into a synthetic counterpart  $\hat{x}$  as follows:

$$\hat{x} = \text{Decoder}(\hat{z}), \quad \text{where} \quad \hat{z} = z + \epsilon_t - \epsilon_\theta(z, t), \quad z = \text{Encoder}(x). \quad (1)$$

where  $z$  represents the encoded latent of the real image, while  $\hat{z}$  is modified by adding noise and subsequently denoising, creating new latents that subtly differ from  $z$ . However, such self-supervised diffusion reconstruction can still lead to changes in image details due to modifications in the latent space, which is responsible for the generation of semantics. The work [33] further simplifies the reconstruction process by using a Variational Autoencoder (VAE)—a submodule used in all stable diffusion generators—without any modification to the latent. This approach generates images that closely match the original real image at the pixel level.

$$\hat{x} = \text{Decoder}(z), \quad \text{where} \quad z = \text{Encoder}(x). \quad (2)$$

**Frequency-Level Misalignment Exists and Can Be Exploited.** Frequency domain has been widely explored in AIGI detectors [37, 23, 30, 48], demonstrating that frequency information is crucial for AIGI detection. This motivates us to revisit the frequency-domain alignment. Surprisingly, despite pixel-level alignment, synthetic counterparts exhibit significant discrepancies in high-frequency content. Figure 4 visualizes this discrepancy between the real image and synthetic images reconstructed using various VAEs. Real images are often with relatively poor high-frequency information, which is due to JPEG compression removing high-frequency details. Having identified this frequency-level discrepancy, another question arises: "Can this disparity be leveraged, or are we overestimating its impact?" To evaluate its effect, we assess the impact by measuring the variance in

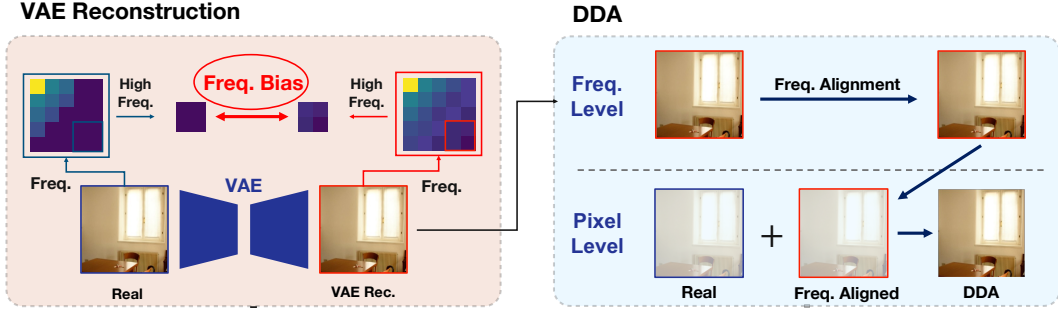


Figure 6: DDA pipeline. **Left:** VAE-reconstructed images differ from real ones in the intensity of high-frequency components. **Right:** DDA fuses high-frequency information from real images into the VAE-reconstructed images to align them in the frequency domain. Then, DDA uses pixel-level mixup of real and frequency-aligned images to further align them in the pixel domain.

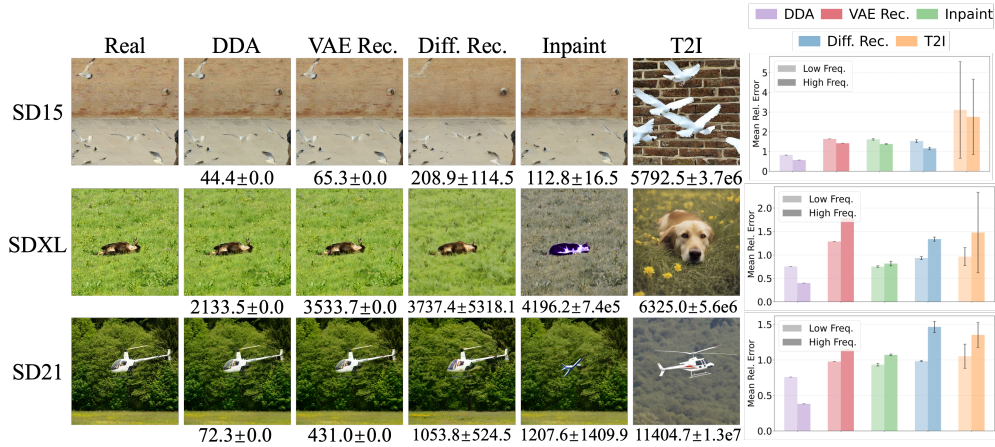


Figure 7: Comparison of various image processing methods based on loss with respect to the real image. **Left:** Comparison of image processing methods across three Stable Diffusion model series (SD15, SDXL, SD21) displaying real images alongside processed versions using DDA, VAE reconstruction (VAE Rec.), diffusion reconstruction (Diff. Rec.), masked inpainting with prompts (Inpaint), and text-to-image generation (T2I). Mean squared error (MSE) values relative to the real image are presented beneath each processed image, and each mse value is calculated by generating 100 images. **Right:** Visualization of relative error metrics for each processing method across the same model series, segregated into low frequency and high frequency bands as calculated using discrete Fourier transform (DFT). Bar charts illustrate comparative error magnitudes across different reconstruction techniques and frequency components. Both pixel-level and frequency-level analyses indicate that DDA produces synthetic images most similar to the real images.

detector performance on VAE-reconstructed images. As shown in Figure 5, the empirical results are striking: visually identical VAE-reconstructed images are detected by the frequency-based detector SAFE [23] with a 93% success rate, indicating a significant difference in the frequency domain. However, when we mask high-frequency information slightly, the detection rate drops dramatically. This substantial decline cannot be attributed solely to information loss; rather, it suggests that detectors exploit biased features—specifically, the richer high-frequency details in synthetic images due to their not undergoing JPEG compression, unlike real images.

### 3.2 Dual Data Alignment

Motivated by the previous observation, we propose DDA, a technique that generates synthetic images aligned with real ones in both the pixel and frequency domains to mitigate the learning of biased features. As illustrated in Figure 6, DDA consists of three steps: 1) **VAE Reconstruction:** Generate

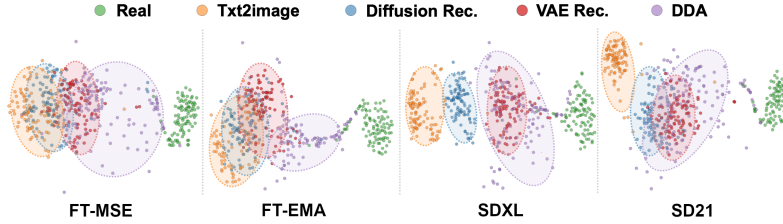


Figure 8: t-SNE visualizations comparing real and generated images, illustrating the proximity of synthetic image cluster centers to real images in feature space. The ordering of proximity—from closest to farthest—is: DDA, VAE reconstruction, diffusion reconstruction, and text-to-image (T2I) generation. These results indicate that DDA produces synthetic samples most closely aligned with real images near the data manifold boundary, thereby facilitating the learning of a tighter and more generalizable decision boundary.

pixel-wise similar images containing VAE-specific artifacts. 2) **Frequency-Level Alignment:** We identified that discrepancies in the frequency domain primarily arise from JPEG compression. To mitigate this, we align the frequency by applying the same JPEG compression with an equivalent quality factor to both real and VAE-reconstructed images. In practice, we estimate the quality factor of each real image before training and apply the same compression to its reconstructed counterpart during training. 3) **Pixel-Level Alignment:** Apply mixup between real and frequency-aligned images to ensure pixel-domain alignment. A closely aligned synthetic image is generated as follow:

$$x_{\text{mix}} = r_{\text{pixel}} \cdot x_{\text{real}} + (1 - r_{\text{pixel}}) \cdot x_{\text{syn}}. \quad (3)$$

where  $r_{\text{pixel}} \in [0, 1]$  controls the degree of pixel-level alignment. A higher  $r_{\text{pixel}}$  value yields a closer synthetic image in the pixel space. In practice,  $r_{\text{pixel}}$  is sampled from a uniform distribution  $\mathcal{U}(0, R_{\text{pixel}})$ . Together, these steps ensure that the resulting synthetic images preserve generative artifacts while maintaining close alignment with real data, both spectrally and spatially.

The generalizability of DDA is built upon two foundations: 1) **VAE artifacts generalize across generators.** Because VAE-reconstructed images are the closest synthetic counterparts to real images, decision boundaries learned from these pairs are likely to remain effective for distinguishing other, more distant synthetic variants (e.g., those from text-to-image generators). Moreover, since the VAE decoder is typically the final stage in diffusion-based generators, its artifacts are less influenced by subsequent modules. 2) **Dual-domain alignment mitigates dataset bias.** By aligning synthetic images with real ones in both the frequency and pixel domains, DDA reduces real-synthetic discrepancies more effectively than alternative reconstruction-based methods. In particular, it eliminates high-frequency bias—commonly introduced by compression or generative artifacts—leading to stronger generalization and reduced reliance on spurious features.

**Comparison to Dataset Alignment Methods.** We validate that DDA creates the closest real-synthetic image pairs when compared to other alignment methods from the following three viewpoints: 1) Pixel domain: Left of Figure 7 shows that DDA-aligned images lead to minimal MSE loss compared to the original image; 2) Frequency domain: Right of Figure 7 shows that DDA-aligned images are most similar to the original image in frequency space; 3) Feature domain: Figure 8 validates that the cluster center of DDA-aligned images is closest to the center of real images.

## 4 Experiments

### 4.1 Experimental Setup

**Datasets** All compared detectors are evaluated on eleven diverse datasets, including seven benchmark datasets (GenImage [59], DRCT-2M [4], Synthbuster [1], DDA-COCO, EvalGEN, AIGCDetectionBenchmark [56] and ForenSynths [43]) and four in-the-wild datasets (Chameleon [48], WildRF [2], SynthWildx [7] and BFree-Online [14]), where images are sourced from the web. These datasets contain real images from different sources and various generators, including diffusion models, GAN models, auto-regressive models, and other unknown models. They differ in format, content, and resolution, thereby minimizing evaluation bias. Table 1 outlines the datasets’ details.

Table 1: Overview of the evaluation benchmarks. “SD” denotes Stable Diffusion and “AR” denotes auto-regressive models. The diversity of data sources and generator types—along with four benchmarks collected from in-the-wild data with unknown generators and post-processing—ensures that the overall evaluation more accurately reflects a detector’s generalizability and practical applicability.

Dataset	Real/Fake	Source	#Models	Model Types
DDA-COCO (ours)	5K/25K	MSCOCO	5	SD
EvalGEN (ours)	0/2765	Prompt	5	SD & AR
GenImage [59]	48K/48K	ImageNet	8	SD & GAN
DRCT-2M [4]	5K/80K	MSCOCO	16	SD
Synthbuster [11]	1K/9K	RAISE	9	SD
AIGCDetectionBenchmark [56]	76.25K/76.25K	LSUN & MSCOCO & ImageNet & CelebA & FFHQ	17	SD & GAN
ForenSynths [43]	36.2K/36.2K	LSUN & MSCOCO & ImageNet & CelebA & others	11	GAN
Chameleon [48]	14.9K/11.2K	Internet	unknown	unknown
WildRF [2]	500/500	Reddit, FB, X	unknown	unknown
SynthWildx [7]	500/1.5K	X	3	SD
BFree-Online [14]	303/641	Internet	unknown	unknown

Table 2: **Overall comparison across 11 benchmarks.** To ensure fairness and reproducibility, we use official checkpoints released by each method. We exclude B-Free [14] from this comparison due to the unavailability of public code. JPEG compression with a quality factor of 96 is applied to the synthetic images in GenImage, ForenSynths, and AIGCDetectionBenchmark to mitigate format bias. The number of generators used in each dataset is reported below the dataset name, where G refers to GANs, D to Diffusion models, and AR to Auto-Regressive models. Bold numbers indicate the best performance per column; underlined numbers indicate the second-best.

Method	Manually Curated Datasets						In-the-Wild Datasets				Avg	Min	
	GenImage 1G + 7D	DRCT-2M 16D	DDA-COCO SD	EvalGEN 3D + 2AR	Synthbuster 9D	ForenSynths 11G	AIGCDetection Benchmark 7G + 10D	Chameleon Unknown	Synthwildx 3D	WildRF Unknown			BFree-Online Unknown
NPR <small>cvpr24</small> [8]	51.5 ± 6.3	37.3 ± 15.0	42.2 ± 5.4	2.9 ± 2.7	50.0 ± 2.6	47.9 ± 22.6	53.1 ± 12.2	59.9	49.8 ± 10.0	63.5 ± 13.6	49.5	46.1 ± 16.1	2.9
UnivFD <small>cvpr26</small> [32]	64.1 ± 10.8	61.8 ± 8.9	52.4 ± 1.5	15.4 ± 14.2	67.8 ± 14.4	77.7 ± 16.1	72.5 ± 17.3	50.7	52.3 ± 11.3	55.3 ± 5.7	49.0	56.3 ± 16.5	15.4
FatFormer <small>cvpr24</small> [31]	62.8 ± 10.4	52.2 ± 5.7	51.7 ± 1.5	45.6 ± 33.1	56.1 ± 10.7	80.0 ± 11.8	85.0 ± 14.9	51.2	52.1 ± 8.2	58.9 ± 8.0	50.0	59.6 ± 14.6	45.6
SAFE <small>cvpr25</small> [23]	50.3 ± 1.2	59.3 ± 19.2	49.9 ± 0.3	1.1 ± 0.6	46.5 ± 20.8	49.7 ± 2.7	50.3 ± 1.1	59.2	49.1 ± 0.7	57.2 ± 18.5	50.5	47.6 ± 16.0	1.1
C2P-CLIP <small>aaar25</small> [38]	74.4 ± 8.4	59.2 ± 9.9	51.3 ± 0.6	38.9 ± 31.2	68.5 ± 11.4	92.9 ± 10.1	81.4 ± 15.6	51.1	57.1 ± 4.2	59.6 ± 7.7	50.0	62.1 ± 15.6	38.9
AIDE <small>cvpr24</small> [48]	61.2 ± 11.9	64.6 ± 11.8	50.0 ± 0.4	19.1 ± 11.1	53.9 ± 18.6	59.4 ± 24.6	63.6 ± 13.9	63.1	48.8 ± 0.8	58.4 ± 12.9	53.1	54.1 ± 12.8	19.1
DRCT <small>icml24</small> [4]	84.7 ± 2.7	90.5 ± 7.4	60.2 ± 4.3	77.8 ± 5.4	84.8 ± 3.6	73.9 ± 13.4	81.4 ± 12.2	56.6	55.1 ± 1.8	50.6 ± 3.5	55.7	70.1 ± 14.6	50.6
AlignedForensics <small>iclr25</small> [33]	79.0 ± 22.7	95.5 ± 6.1	86.5 ± 19.1	68.0 ± 20.7	77.4 ± 25.0	53.9 ± 7.1	66.6 ± 21.6	71.0	78.8 ± 17.8	80.1 ± 10.3	68.5	75.0 ± 11.1	53.9
<b>DDA (ours)</b>	<b>91.7 ± 7.8</b>	<b>98.1 ± 1.4</b>	<b>92.2 ± 10.6</b>	<b>97.2 ± 4.2</b>	<b>90.1 ± 5.6</b>	81.4 ± 13.9	<b>87.8 ± 12.6</b>	<b>82.4</b>	<b>90.9 ± 3.1</b>	<b>90.3 ± 3.5</b>	<b>95.1</b>	<b>90.7 ± 5.3</b>	<b>81.4</b>

**DDA-COCO and EvalGEN** DDA-COCO consists of five subsets containing reconstructed images of MSCOCO [28] validation set by different VAEs, utilizing frequency-level alignment. We construct the EvalGEN dataset using the five latest text-to-image (T2I) generators using aligned prompts from the GenEval benchmark [11]. Notably, **we are the first work to involve auto-regressive-based T2I generators for image forensics in the AIGI detection field.** Specifically, we introduce each generator as follows: (1) **Flux** [22]: the SOTA diffusion-based generator, offering extremely higher-resolution output images. (2) **GoT** [10]: A multimodal model combining LLM and diffusion processes to enable reasoning-guided image generation. (3) **Infinity** [16]: A bitwise auto-regressive model using infinite-vocabulary tokenization and self-correction for faster and higher-fidelity image generation. (4) **OmiGen** [44]: A unified multimodal framework capable of handling diverse image generation tasks within a single, simplified architecture. (5) **NOVA** [9]: A non-quantized auto-regressive model designed for efficient image and video generation, achieving high fidelity with reduced computational overhead. These models allow our **EvalGEN to serve as a very high-quality benchmark** for evaluating the generalizability of detectors on unseen generators.

**Implementation Details** We use DINOv2 as the backbone and fine-tune it with LoRA, using a rank of 8. The input resolution is set to 336×336, employing random cropping during training and center cropping during validation. Padding is applied when the image height or width is insufficient. The training data exclusively consists of MSCOCO [29] images and their DDA-aligned counterparts. During VAE reconstruction, to ensure that the reconstructed image size matches the real one, we first center-crop each image to the largest size that is a multiple of 8, following the VAE model’s design. For frequency alignment in DDA, we apply the same JPEG compression to each reconstructed counterpart with a 50% probability during training, allowing the model to encounter both JPEG and PNG formats of synthetic images. *All evaluations are conducted using a single model without any dataset-specific fine-tuning or threshold adjustments.*

**Evaluation Metrics and Comparative Methods** Unless otherwise specified, we report balanced accuracy, the average of real and fake accuracies, as the evaluation metric, following works [8, 32, 31, 23, 38, 48, 4, 33, 14]. The methods compared include four frequency-based detectors: NPR [8], SAFE [23], and AIDE [48]; three CLIP-based detectors: UnivFD [32], FatFormer [31], and C2P-CLIP [38]; and two data alignment methods: DRCT [4] and AlignedForensics [33].

Table 3: Comparison of balanced accuracy between DDA and compared methods on DRCT-2M.

Method	LDM	SDv1.4	SDv1.5	SDv2	SDXL	SDXL-Retiner	SD-Turbo	SDXL-Turbo	LCM-SDv1.5	LCM-SDXL	SDv1-Ctrl	SDv2-Ctrl	SDXL-Ctrl	SDv1-DR	SDv2-DR	SDXL-DR	Avg.
NPR (CVPR'24) [8]	33.0	29.1	29.0	35.1	33.2	28.4	27.9	27.9	29.4	30.2	28.4	28.3	34.7	67.9	67.4	66.1	37.3 ± 15.0
UnivFD (CVPR'23) [32]	35.4	36.8	36.4	38.2	63.2	55.0	56.5	53.0	54.5	65.9	68.0	65.4	75.9	64.6	56.2	53.9	61.8 ± 8.9
FatFormer (CVPR'24) [31]	55.9	48.2	48.2	48.2	48.2	48.3	48.2	48.2	48.3	50.6	49.7	49.9	59.8	66.3	60.6	56.0	52.2 ± 5.7
SAFE (KDD'25) [23]	50.3	50.1	50.0	50.0	49.9	50.1	50.0	50.0	50.1	50.0	49.9	50.0	54.7	98.2	98.5	97.3	59.3 ± 19.2
C2P-CLIP (AAAI'25) [38]	83.0	51.7	51.7	52.9	51.9	64.6	51.7	50.6	52.0	66.1	56.9	54.7	77.8	67.2	57.1	56.7	59.2 ± 9.9
AIDE (ICLR'25) [48]	64.4	74.9	75.1	58.5	53.5	66.3	52.8	52.8	70.0	54.3	65.9	53.6	53.9	95.3	73.3	69.0	64.6 ± 11.8
DRCT (ICML'24) [4]	96.7	96.3	96.3	94.9	96.2	93.5	93.4	92.9	91.2	95.0	95.6	92.7	92.0	94.1	69.6	57.4	90.5 ± 7.4
AlignedForensics (ICLR'25) [33]	<b>99.9</b>	<b>99.9</b>	<b>99.9</b>	<b>99.6</b>	90.2	81.3	<b>99.7</b>	89.4	<b>99.7</b>	90.0	<b>99.9</b>	<b>99.2</b>	87.6	<b>99.9</b>	<b>99.8</b>	92.6	<b>95.3 ± 6.1</b>
<b>DDA (ours)</b>	<b>99.2</b>	<b>98.9</b>	<b>99.0</b>	<b>98.3</b>	<b>98.0</b>	<b>96.8</b>	<b>97.9</b>	<b>94.8</b>	<b>95.9</b>	<b>98.2</b>	<b>98.7</b>	<b>99.0</b>	<b>99.4</b>	<b>99.0</b>	<b>99.5</b>	<b>96.3</b>	<b>98.1 ± 1.4</b>

Table 4: Comparison of balanced accuracy on GenImage.

Method	Midjourney	SDv1.4	SDv1.5	ADM	GLIDE	Wukong	VQDM	BigGAN	Avg.
NPR (CVPR'24) [8]	53.4	55.1	55.0	43.8	41.2	57.4	48.4	57.7	51.5 ± 6.3
UnivFD (CVPR'23) [32]	55.1	55.6	55.7	62.5	61.3	61.1	76.9	84.4	64.1 ± 10.8
FatFormer (CVPR'24) [31]	52.1	53.6	53.8	61.4	65.5	60.9	72.5	82.2	62.8 ± 10.4
SAFE (KDD'25) [23]	49.0	49.7	49.8	49.5	53.0	50.3	50.2	50.9	50.3 ± 1.2
C2P-CLIP (AAAI'25) [38]	56.6	77.5	76.9	71.6	73.5	79.4	73.7	85.9	74.4 ± 8.4
SAFE (ICLR'25) [48]	58.2	77.2	77.4	50.4	54.6	70.5	50.8	50.6	61.2 ± 11.9
DRCT (ICML'24) [4]	82.4	88.3	88.2	76.9	86.1	87.9	<b>85.4</b>	<b>87.0</b>	<b>84.7 ± 2.7</b>
AlignedForensics (ICLR'25) [33]	<b>97.5</b>	<b>99.7</b>	<b>99.6</b>	52.4	57.6	<b>99.6</b>	75.0	50.6	79.0 ± 22.7
<b>DDA (ours)</b>	<b>95.6</b>	<b>98.7</b>	<b>98.6</b>	<b>89.5</b>	<b>89.6</b>	<b>98.7</b>	76.5	<b>86.5</b>	<b>91.7 ± 7.8</b>

Table 5: Comparison of balanced accuracy on AIGCDetectionBenchmark.

Method	ADM	DALLE2	GLIDE	Midjourney	VQDM	BigGAN	CycleGAN	GauGAN	ProGAN	SDXL	SDH	SD15	StarGAN	StyleGAN	StyleGAN2	WFR	Wukong	Avg.
NPR (CVPR'24) [8]	43.8	20.0	41.2	53.4	48.4	53.1	76.6	42.2	58.7	99.6	55.1	55.0	67.4	37.9	34.6	58.8	57.4	51.1 ± 12.2
UnivFD (CVPR'23) [32]	62.5	50.0	61.3	55.1	54.4	58.0	<b>99.2</b>	<b>99.5</b>	<b>99.1</b>	98.5	71.7	67.5	67.2	<b>99.4</b>	<b>98.0</b>	69.4	61.1	72.5 ± 17.3
FatFormer (CVPR'24) [31]	<b>99.3</b>	68.5	<b>91.1</b>	49.0	<b>99.2</b>	52.1	51.9	50.0	49.8	49.7	49.8	50.1	50.0	50.0	<b>98.8</b>	<b>88.1</b>	75.6	<b>85.0 ± 14.9</b>
SAFE (KDD'25) [23]	49.5	49.5	53.0	49.0	50.2	52.1	51.9	50.0	50.0	49.8	49.7	49.8	50.1	50.0	50.0	49.8	50.3	50.3 ± 1.4
C2P-CLIP (AAAI'25) [38]	71.6	52.3	73.5	56.6	73.7	58.4	96.8	58.2	59.3	62.3	77.5	76.9	<b>99.6</b>	93.1	79.4	<b>94.8</b>	79.4	81.4 ± 15.6
AIDE (ICLR'25) [48]	52.9	51.1	60.2	49.8	69.3	70.1	93.6	60.9	89.0	49.6	51.6	51.0	72.1	66.3	59.0	80.6	54.5	45.6 ± 13.9
DRCT (ICML'24) [4]	79.9	89.2	89.2	85.5	<b>88.6</b>	81.4	91.0	91.8	88.3	91.4	91.0	53.0	62.7	63.8	73.9	90.8	81.4 ± 12.2	
AlignedForensics (ICLR'25) [33]	51.6	52.0	55.6	<b>96.2</b>	72.1	51.2	49.5	50.8	50.7	<b>95.1</b>	<b>99.7</b>	<b>99.6</b>	53.8	52.7	51.6	50.0	<b>99.6</b>	66.6 ± 21.6
<b>DDA (ours)</b>	<b>89.5</b>	<b>94.6</b>	<b>88.6</b>	<b>95.6</b>	76.6	91.0	72.5	92.7	<b>92.8</b>	<b>99.4</b>	<b>98.2</b>	<b>98.6</b>	72.7	87.8	<b>90.4</b>	52.1	<b>98.8</b>	<b>87.8 ± 12.6</b>

Table 6: Comparison of balanced accuracy between DDA and compared methods on ForenSynths.

Method	BigGAN	CRN	CycleGAN	DeepFake	GauGAN	IMLE	ProGAN	SAN	SeeingDark	StarGAN	StyleGAN	StyleGAN 2	WFR	Avg.
NPR (CVPR'24) [8]	53.1	0.4	76.6	35.7	42.2	5.3	58.7	48.4	63.6	67.4	57.9	54.6	58.8	47.9 ± 22.6
UnivFD (CVPR'23) [32]	87.5	55.7	96.9	69.4	98.8	68.1	<b>99.4</b>	58.2	62.2	95.1	80.0	69.4	69.2	77.7 ± 16.1
FatFormer (CVPR'24) [31]	<b>99.3</b>	72.1	<b>99.5</b>	<b>93.0</b>	<b>99.3</b>	72.1	98.4	70.8	81.9	<b>99.4</b>	<b>98.1</b>	<b>98.9</b>	<b>88.3</b>	<b>90.1 ± 11.8</b>
SAFE (KDD'25) [23]	52.2	50.0	51.9	50.1	50.0	50.0	50.0	50.9	41.1	50.1	50.0	50.0	49.8	49.7 ± 2.7
C2P-CLIP (AAAI'25) [38]	98.4	<b>93.3</b>	96.8	92.6	98.8	<b>93.2</b>	<b>99.3</b>	63.2	<b>94.7</b>	<b>99.6</b>	93.1	79.4	<b>94.8</b>	<b>92.1 ± 10.1</b>
AIDE (ICLR'25) [48]	70.1	12.2	93.6	53.2	60.6	15.9	89.0	55.3	44.2	72.1	66.5	59.0	80.6	59.4 ± 24.6
DRCT (ICML'24) [4]	81.4	78.4	91.0	51.5	93.8	82.6	71.1	84.9	72.2	53.0	62.7	63.8	73.9	73.9 ± 13.4
AlignedForensics (ICLR'25) [33]	51.2	50.4	49.5	71.7	50.8	49.7	50.7	67.6	51.4	53.8	52.7	51.6	50.0	53.9 ± 7.1
<b>DDA (ours)</b>	91.0	<b>87.0</b>	72.5	76.5	92.7	<b>89.7</b>	92.8	<b>94.7</b>	58.6	72.7	87.8	<b>90.2</b>	52.1	81.4 ± 13.9

## 4.2 Cross-Dataset and Cross-Model Comparison

**Overall Comparison on 11 Benchmarks.** Table 2 presents a comprehensive comparison across 11 datasets—7 manually curated and 4 in-the-wild—covering most known open-source AIGI evaluation benchmarks. To the best of our knowledge, the first large-scale comparison of its kind. As benchmarks vary greatly, the benefits of exploiting any bias are minimized, making the average accuracy across the 11 benchmarks more representative of the detector’s practical performance. The results show that: 1) DDA achieves an average accuracy of 90.7%, marking a 15.7% improvement over the second-best method. Notably, DDA reaches 82.4% accuracy on the challenging Chameleon benchmark, where only AlignedForensics achieves above 70%; 2) DDA also has the highest minimal accuracy of 81.4%, significantly outperforming the second-best method by 27.5%. Moreover, DDA exhibits the smallest deviation across benchmarks, less than half of the other methods, suggesting it is more reliable and robust; 3) An interesting observation is that, when comparing methods across datasets, detectors trained on more aligned data tend to achieve much higher average accuracy. The degree of data alignment in the detectors, in increasing order, is as follows: UnivFD (no data alignment), DRCT (data alignment via diffusion reconstruction), AlignedForensics (data alignment via VAE reconstruction), and DDA (dual-domain data alignment). The overall average accuracy follows the same order as the degree of data alignment. This clearly demonstrates the effectiveness of data alignment in improving a detector’s generalizability, supporting our previous assertion that data alignment helps models learn more transferable decision boundaries.

**Detailed Comparison on DRCT-2M, GenImage, AIGCDetectionBenchmark, ForenSynths, Synthbuster, SynthWildx, and WildRF.** Table 3 to Table 8 report the detailed performance of various methods across these subsets. From the results, we observe the following: (1) Consistent superiority: DDA not only surpasses other detectors by a substantial margin in average accuracy (ranging from 3% to 10%) but also achieves consistently lower deviations across all benchmarks. Given the diversity of real image sources and the inclusion of both GAN- and diffusion-based models,

Table 7: Comparison of balanced accuracy between DDA and compared methods on Synthbuster.

Method	DALL-E 2	DALL-E 3	Firefly	GLIDE	Midjourney	SD 1.3	SD 1.4	SD 2	SDXL	Avg.
NPR (CVPR'24) [8]	51.1	49.3	46.5	48.5	52.8	51.4	51.8	46.0	52.8	50.0 ± 2.6
UnivFD (CVPR'23) [32]	<u>83.5</u>	47.4	<u>89.9</u>	53.3	52.5	70.4	69.9	75.7	68.0	67.8 ± 14.4
FatFormer (CVPR'24) [31]	59.4	39.5	60.3	72.7	44.4	53.7	54.0	52.3	69.1	56.1 ± 10.7
SAFE (KDD'25) [23]	58.0	9.9	10.3	52.2	56.7	59.4	59.1	53.0	59.5	46.5 ± 20.8
C2P-CLIP (AAAI'25) [38]	55.6	63.2	59.5	<b>86.7</b>	52.9	75.2	76.7	69.2	77.7	68.5 ± 11.4
AIDE (ICLR'25) [48]	34.9	33.7	24.8	65.0	57.5	74.1	73.7	53.2	68.4	53.9 ± 18.6
DRCT (ICML'24) [4]	77.2	<u>86.6</u>	84.1	<u>82.6</u>	73.7	86.6	86.6	83.2	71.3	<u>84.8</u> ± 3.6
AlignedForensics (ICLR'25) [33]	50.2	48.9	51.7	53.5	<b>98.7</b>	<b>98.8</b>	<b>98.8</b>	<b>98.6</b>	<b>97.3</b>	77.4 ± 25.0
<b>DDA (ours)</b>	<b>86.3</b>	<b>90.0</b>	<b>91.9</b>	76.5	<u>93.5</u>	<u>92.9</u>	<u>92.7</u>	<u>93.3</u>	<u>93.5</u>	<b>90.1</b> ± 5.6

Table 8: Comparison of balanced accuracy between DDA and compared methods on SynthWildx and WildRF.

Method	SynthWildx				WildRF			
	DALL-E 3	Firefly	Midjourney	Avg.	Facebook	Reddit	Twitter	Avg.
NPR (CVPR'24) [8]	43.6	61.3	44.5	49.8 ± 10.0	78.1	61.0	51.3	63.5 ± 13.6
UnivFD (CVPR'23) [32]	45.4	<u>65.3</u>	46.2	52.3 ± 11.3	49.1	60.2	56.5	55.3 ± 5.7
FatFormer (CVPR'24) [31]	46.5	61.6	48.3	52.1 ± 8.2	54.1	68.1	54.4	58.9 ± 8.0
SAFE (KDD'25) [23]	49.4	48.2	49.6	49.1 ± 0.7	50.9	<u>74.1</u>	37.5	57.2 ± 18.5
C2P-CLIP (AAAI'25) [38]	56.9	61.4	53.0	57.1 ± 4.2	54.4	68.4	55.9	59.6 ± 7.7
AIDE (ICLR'25) [48]	63.4	48.8	51.9	48.8 ± 0.8	57.8	71.5	45.8	58.4 ± 12.9
DRCT (ICML'24) [4]	58.3	56.4	50.5	55.1 ± 1.8	46.6	53.1	55.2	50.6 ± 3.5
AlignedForensics (ICLR'25) [33]	<u>85.5</u>	58.5	<u>92.2</u>	78.8 ± 17.8	89.4	69.1	81.8	<u>80.1</u> ± 10.3
<b>DDA (ours)</b>	<b>92.3</b>	<b>87.3</b>	<b>93.1</b>	<b>90.9</b> ± 3.1	<b>93.1</b>	<b>86.4</b>	<b>91.5</b>	<b>90.3</b> ± 3.5

Table 9: Comparison of balanced accuracy between our DDA and other methods on DDA-COCO.

Method	real	fake						Avg
		XL	EMA	MSE	SD21	SD35	FLUX.1	
NPR (CVPR'24) [8]	55.4	16.1	31.1	41.3	41.2	24.9	19.2	42.2 ± 5.4
UnivFD (CVPR'23) [32]	99.2	3.9	9.6	7.3	7.4	3.4	1.8	52.4 ± 1.5
FatFormer (CVPR'24) [31]	96.4	5.4	6.9	10.4	10.3	6.6	2.8	51.7 ± 1.5
SAFE (KDD'25) [23]	98.8	0.6	0.9	0.9	1.0	0.3	1.8	49.9 ± 0.3
C2P-CLIP (AAAI'25) [38]	99.5	2.0	2.7	4.3	4.2	4.0	1.3	51.3 ± 0.6
AIDE (ICLR'25) [48]	98.8	0.6	2.2	1.7	1.8	0.3	0.6	50.0 ± 0.4
DRCT (ICML'24) [4]	94.2	16.9	34.8	33.3	33.6	21.7	17.2	60.2 ± 4.3
AlignedForensics (ICLR'25) [33]	<b>99.8</b>	<b>82.5</b>	<b>99.2</b>	<b>99.0</b>	<b>99.1</b>	<b>55.4</b>	<b>3.6</b>	<b>86.5</b> ± 19.1
<b>DDA (ours)</b>	99.0	<b>95.0</b>	<b>99.3</b>	<b>99.7</b>	<b>99.7</b>	<b>68.1</b>	<b>50.2</b>	<b>92.2</b> ± 10.6

Table 10: Comparison of balanced accuracy on EvalGEN.

Method	Flux	GoT	Infinity	NOVA	OmniGen	Avg.
NPR (CVPR'24) [8]	0.7	0.2	6.5	4.7	2.2	2.9 ± 2.7
UnivFD (CVPR'23) [32]	4.0	9.2	15.7	8.3	39.6	15.4 ± 14.2
FatFormer (CVPR'24) [31]	9.9	47.9	44.7	<u>98.3</u>	27.3	45.6 ± 33.1
SAFE (KDD'25) [23]	1.0	0.5	1.9	0.6	1.6	1.1 ± 0.6
C2P-CLIP (AAAI'25) [38]	8.7	49.6	35.3	86.4	14.5	38.9 ± 31.2
AIDE (ICLR'25) [48]	17.9	24.7	3.4	16.3	33.4	19.1 ± 11.1
DRCT (ICML'24) [4]	72.5	81.4	72.9	84.6	77.8	77.8 ± 5.4
AlignedForensics (ICLR'25) [33]	32.0	72.3	74.0	84.8	71.0	68.0 ± 20.7
<b>DDA (ours)</b>	<b>89.9</b>	<b>99.5</b>	<b>97.8</b>	<b>99.5</b>	<b>90.5</b>	<b>97.2</b> ± 4.2

these results strongly demonstrate the effectiveness and generalizability of DDA. (2) Exception on ForenSynths: DDA underperforms slightly on the ForenSynths benchmark. We attribute this to the fact that the two methods outperforming DDA—FatFormer and C2P-CLIP—were trained on ProGAN, which is also the generator used in the ForenSynths subsets, giving them an advantage. Moreover, some data in the ForenSynths are generated by older and smaller models, which deviate significantly from modern generators, contributing to DDA’s performance degradation.

**Comparison on DDA-COCO and EvalGEN** Table 9 and Table 10 report accuracies on our two proposed benchmarks, DDA-COCO and EvalGEN, respectively. We observe the following: (1) Generalization across diffusion models: DDA, trained solely on SD 2.1–reconstructed data, generalizes well to other diffusion models and exhibits a smaller standard deviation. This suggests that DDA learns a universal upsampling artifact shared across diverse generative models, reinforcing our claim that data alignment enhances generalizability. (2) Effectiveness of data alignment: Results on DDA-COCO highlight the importance of data alignment. Methods lacking explicit alignment—such as NPR [8], UnivFD [32], FatFormer [31], C2P-CLIP [38], AIDE [48], and SAFE [23]—exhibit large disparities between real and fake accuracies, revealing underlying dataset biases. (3) Performance on emerging generators: DDA also achieves SOTA on EvalGEN, excelling on auto-regressive generators, further validating its strong cross-architecture generalizability.

**Comparison on Generation Time Cost** We compare three methods which introduce train data generation—DRCT [4], AlignedForensics [33], and B-Free [14]. Table 11 presents the number of real and synthetic images used for training, generation method and the estimated reconstruction time (Single Image & Full Set) using each method, which is tested by generating 100 synthetic images. Results show that our DDA requires the least amount of training data and reconstruction time, confirming its effectiveness and efficiency in terms of training cost.

Table 11: Comparing on data generation time.

Method	# Real / Fake	Generation Method	Time Per Image	Full Construction Time
DRCT	118K / 354K	Diff. Rec.	0.6569 ± 0.0050 s	64.6 h
AlignedForensics	179K / 179K	VAE Rec.	0.1756 ± 0.0692 s	8.73 h
B-Free	51K / 309K	Diff. Rec + Inpaint.	3.0150 ± 0.0125 s	258.79 h
<b>DDA (ours)</b>	<b>118K / 118K</b>	<b>VAE Rec. + DDA</b>	<b>0.1792 ± 0.0704 s</b>	<b>5.9 h</b>

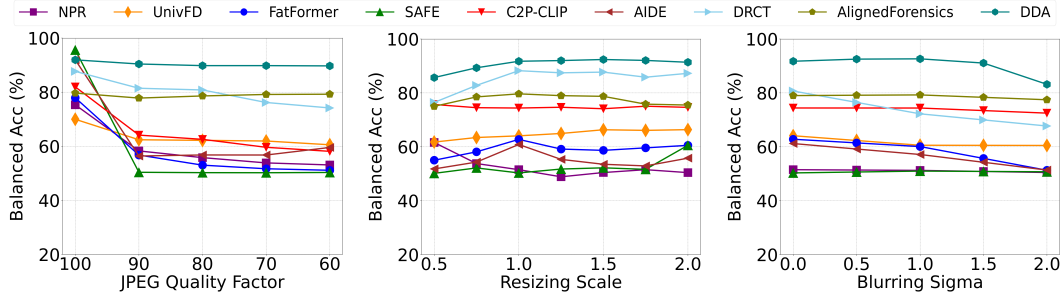


Figure 9: Robustness analysis on GenImage.

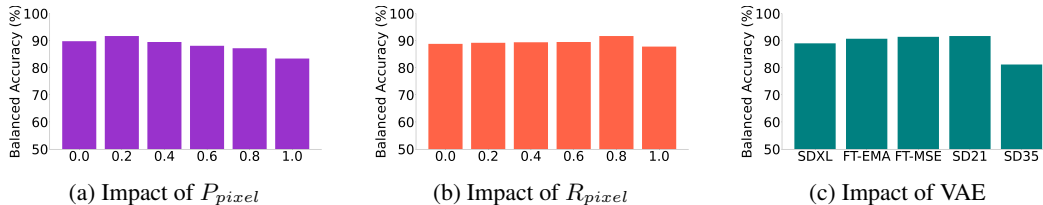


Figure 10: **Ablation studies.** (a)  $P_{pixel}$ : probability of applying pixel-level alignment; (b)  $R_{pixel}$ : upper bound for sampling the pixel mixup ratio; (c) VAE: backbone used for training data reconstruction. Results show the impact of each hyperparameter on the performance of DDA.

### 4.3 Evaluation on Robustness

Figure 9 shows the results of three robustness evaluations on the GenImage-JPEG96 dataset for all compared methods. Results show that: (1) DDA shows strong robustness across all three post-processing methods, outperforming the second-best method by 10.5%, 4.1%, and 5.7% under JPEG 60, RESIZE 2.0, and BLUR 2.0, respectively. (2) Methods lacking alignment, such as NPR [8], SAFE [23], and AIDE [48], demonstrate poor robustness under JPEG compression and resizing. In contrast, methods with alignment perform much better, emphasizing the importance of data alignment.

### 4.4 Ablation Studies

Figure 10 illustrates the impact of  $P_{pixel}$ ,  $R_{pixel}$ , and the choice of VAE in training data generation. Results indicate that the detector maintains consistent accuracy when  $P_{pixel}$  and  $R_{pixel}$  are between 0.2 and 0.8, with performance drops observed at 0.0 and 1.0. Experiments with different VAEs confirm that SD21 is the most effective choice.

## 5 Conclusion

In this paper, we demonstrate that pixel-domain alignment alone is insufficient for fully aligning real and synthetic image pairs. Building on this, we propose DDA to align synthetic images with real ones across both pixel and frequency domains, thereby mitigating bias. We also introduce two AIGI benchmarks: DDA-COCO and EvalGEN. Extensive experiments across eleven benchmarks demonstrate the consistent superiority of DDA. We believe that DDA, DDA-COCO, and EvalGEN provide a solid foundation for advancing the generalization of AIGI detection.

**Limitations and Future Work** While DDA demonstrates strong performance across extensive benchmarks, there remains a gap in its application to real-world scenarios, particularly due to the heavy post-processing applied to images in such contexts. In practice, we observe that even authentic photos taken by smartphones may exhibit synthetic-like artifacts, likely resulting from the AI-based enhancements embedded in modern smartphone camera pipelines, which adds complexity to real-world AIGI detection. In future work, we plan to develop a more practical AIGI detector tailored to address these real-world challenges.

## 6 Acknowledgements

The authors would like to express our sincere gratitude to NeurIPS anonymous reviewers for their constructive feedback. This work is supported by the National Natural Science Foundation of China under Grant 62572188 and Grant 62272164.

## References

- [1] Quentin Bammey. Synthbuster: Towards detection of diffusion model generated images. *IEEE Open Journal of Signal Processing*, 5:1–9, 2023.
- [2] Bar Cavia, Eliahu Horwitz, Tal Reiss, and Yedid Hoshen. Real-time deepfake detection in the real-world. *arXiv preprint arXiv:2406.09398*, 2024.
- [3] George Cazenavette, Avneesh Sud, Thomas Leung, and Ben Usman. Fakeinversion: Learning to detect images from unseen text-to-image models by inverting stable diffusion. In *Proceedings of the IEEE/CVF Conference on Computer Vision and Pattern Recognition*, pages 10759–10769, 2024.
- [4] Baoying Chen, Jishen Zeng, Jianquan Yang, and Rui Yang. Drct: Diffusion reconstruction contrastive training towards universal detection of diffusion generated images. In *Forty-first International Conference on Machine Learning*, 2024.
- [5] Yize Chen, Zhiyuan Yan, Guangliang Cheng, Kangran Zhao, Siwei Lyu, and Baoyuan Wu. X2-dfd: A framework for explainable and extendable deepfake detection. *arXiv preprint arXiv:2410.06126*, 2024.
- [6] Beilin Chu, Xuan Xu, Xin Wang, Yufei Zhang, Weike You, and Linna Zhou. Fire: Robust detection of diffusion-generated images via frequency-guided reconstruction error. In *CVPR*, 2025.
- [7] Davide Cozzolino, Giovanni Poggi, Riccardo Corvi, Matthias Nießner, and Luisa Verdoliva. Raising the bar of ai-generated image detection with clip. In *Proceedings of the IEEE/CVF Conference on Computer Vision and Pattern Recognition*, pages 4356–4366, 2024.
- [8] Davide Cozzolino, Giovanni Poggi, Matthias Nießner, and Luisa Verdoliva. Zero-shot detection of ai-generated images. In *European Conference on Computer Vision*, pages 54–72. Springer, 2024.
- [9] Haoge Deng, Ting Pan, Haiwen Diao, Zhengxiong Luo, Yufeng Cui, Huchuan Lu, Shiguang Shan, Yonggang Qi, and Xinlong Wang. Autoregressive video generation without vector quantization. *arXiv preprint arXiv:2412.14169*, 2024.
- [10] Rongyao Fang, Chengqi Duan, Kun Wang, Linjiang Huang, Hao Li, Shilin Yan, Hao Tian, Xingyu Zeng, Rui Zhao, Jifeng Dai, et al. Got: Unleashing reasoning capability of multimodal large language model for visual generation and editing. *arXiv preprint arXiv:2503.10639*, 2025.
- [11] Dhruva Ghosh, Hannaneh Hajishirzi, and Ludwig Schmidt. Geneval: An object-focused framework for evaluating text-to-image alignment. *Advances in Neural Information Processing Systems*, 36:52132–52152, 2023.
- [12] Ian J Goodfellow et al. Generative adversarial nets. In *Advances in Neural Information Processing Systems*, 2014.
- [13] Patrick Grommelt, Louis Weiss, Franz-Josef Pfreundt, and Janis Keuper. Fake or jpeg? revealing common biases in generated image detection datasets. *arXiv preprint arXiv:2403.17608*, 2024.
- [14] Fabrizio Guillaro, Giada Zingarini, Ben Usman, Avneesh Sud, Davide Cozzolino, and Luisa Verdoliva. A bias-free training paradigm for more general ai-generated image detection. *arXiv preprint arXiv:2412.17671*, 2024.
- [15] Seoyeon Gye, Junwon Ko, Hyounguk Shon, Minchan Kwon, and Junmo Kim. Sfld: Reducing the content bias for ai-generated image detection. *arXiv preprint arXiv:2502.17105*, 2025.

- [16] Jian Han, Jinlai Liu, Yi Jiang, Bin Yan, Yuqi Zhang, Zehuan Yuan, Bingyue Peng, and Xiaobing Liu. Infinity: Scaling bitwise autoregressive modeling for high-resolution image synthesis. *arXiv preprint arXiv:2412.04431*, 2024.
- [17] Xinan He, Yue Zhou, Bing Fan, Bin Li, Guopu Zhu, and Feng Ding. VIforgery face triad: Detection, localization and attribution via multimodal large language models. *arXiv preprint arXiv:2503.06142*, 2025.
- [18] Jonathan Ho et al. Denoising diffusion probabilistic models. *Advances in Neural Information Processing Systems*, 33:6840–6851, 2020.
- [19] Dimitrios Karageorgiou, Symeon Papadopoulos, Ioannis Kompatsiaris, and Efstratios Gavves. Any-resolution ai-generated image detection by spectral learning. In *CVPR*, 2025.
- [20] Tero Karras et al. Progressive growing of gans for improved quality, stability, and variation. In *International Conference on Learning Representations*, 2018.
- [21] Tero Karras et al. A style-based generator architecture for generative adversarial networks. In *Proceedings of the IEEE/CVF Conference on Computer Vision and Pattern Recognition*, pages 4401–4410, 2019.
- [22] Black Forest Labs. Flux. <https://github.com/black-forest-labs/flux>, 2024.
- [23] Ouxiang Li, Jiayin Cai, Yanbin Hao, Xiaolong Jiang, Yao Hu, and Fuli Feng. Improving synthetic image detection towards generalization: An image transformation perspective. *arXiv preprint arXiv:2408.06741*, 2024.
- [24] Ziqiang Li, Jiazhen Yan, Ziwen He, Kai Zeng, Weiwei Jiang, Lizhi Xiong, and Zhangjie Fu. Is artificial intelligence generated image detection a solved problem? *arXiv preprint arXiv:2505.12335*, 2025.
- [25] Kaiqing Lin, Yuzhen Lin, Weixiang Li, Taiping Yao, and Bin Li. Standing on the shoulders of giants: Reprogramming visual-language model for general deepfake detection. In *Proceedings of the AAAI Conference on Artificial Intelligence*, volume 39, pages 5262–5270, 2025.
- [26] Kaiqing Lin, Zhiyuan Yan, Ruoxin Chen, Junyan Ye, Ke-Yue Zhang, Yue Zhou, Peng Jin, Bin Li, Taiping Yao, and Shouhong Ding. Seeing before reasoning: A unified framework for generalizable and explainable fake image detection. *arXiv preprint arXiv:2509.25502*, 2025.
- [27] Kaiqing Lin, Zhiyuan Yan, Ke-Yue Zhang, Li Hao, Yue Zhou, Yuzhen Lin, Weixiang Li, Taiping Yao, Shouhong Ding, and Bin Li. Guard me if you know me: Protecting specific face-identity from deepfakes. *arXiv preprint arXiv:2505.19582*, 2025.
- [28] Tsung-Yi Lin et al. Microsoft coco: Common objects in context. In *European Conference on Computer Vision*, pages 740–755. Springer, 2014.
- [29] Tsung-Yi Lin, Michael Maire, Serge Belongie, James Hays, Pietro Perona, Deva Ramanan, Piotr Dollár, and C Lawrence Zitnick. Microsoft coco: Common objects in context. In *Computer vision—ECCV 2014: 13th European conference, zurich, Switzerland, September 6-12, 2014, proceedings, part v 13*, pages 740–755. Springer, 2014.
- [30] Honggu Liu et al. Spatial-phase shallow learning: rethinking face forgery detection in frequency domain. In *Proceedings of the IEEE/CVF Conference on Computer Vision and Pattern Recognition*, pages 772–781, 2021.
- [31] Huan Liu, Zichang Tan, Chuangchuang Tan, Yunchao Wei, Jingdong Wang, and Yao Zhao. Forgery-aware adaptive transformer for generalizable synthetic image detection. In *Proceedings of the IEEE/CVF Conference on Computer Vision and Pattern Recognition*, pages 10770–10780, 2024.
- [32] Utkarsh Ojha et al. Towards universal fake image detectors that generalize across generative models. In *Proceedings of the IEEE/CVF Conference on Computer Vision and Pattern Recognition*, pages 24480–24489, 2023.

- [33] Anirudh Sundara Rajan, Utkarsh Ojha, Jedidiah Schloesser, and Yong Jae Lee. Aligned datasets improve detection of latent diffusion-generated images, 2025.
- [34] Robin Rombach et al. High-resolution image synthesis with latent diffusion models. In *Proceedings of the IEEE/CVF Conference on Computer Vision and Pattern Recognition*, pages 10684–10695, 2022.
- [35] Zeyang Sha, Zheng Li, Ning Yu, and Yang Zhang. De-fake: Detection and attribution of fake images generated by text-to-image generation models. In *Proceedings of the 2023 ACM SIGSAC conference on computer and communications security*, pages 3418–3432, 2023.
- [36] Yiren Song, Shengtao Lou, Xiaokang Liu, Hai Ci, Pei Yang, Jiaming Liu, and Mike Zheng Shou. Anti-reference: Universal and immediate defense against reference-based generation. *arXiv preprint arXiv:2412.05980*, 2024.
- [37] Chuangchuang Tan et al. Learning on gradients: Generalized artifacts representation for gan-generated images detection. In *Proceedings of the IEEE/CVF Conference on Computer Vision and Pattern Recognition (CVPR)*, pages 12105–12114, June 2023.
- [38] Chuangchuang Tan, Renshuai Tao, Huan Liu, Guanghua Gu, Baoyuan Wu, Yao Zhao, and Yunchao Wei. C2p-clip: Injecting category common prompt in clip to enhance generalization in deepfake detection. In *Proceedings of the AAAI Conference on Artificial Intelligence*, 2024.
- [39] Chuangchuang Tan, Yao Zhao, Shikui Wei, Guanghua Gu, Ping Liu, and Yunchao Wei. Frequency-aware deepfake detection: Improving generalizability through frequency space domain learning. In *Proceedings of the AAAI Conference on Artificial Intelligence*, volume 38, pages 5052–5060, 2024.
- [40] Chuangchuang Tan, Yao Zhao, Shikui Wei, Guanghua Gu, Ping Liu, and Yunchao Wei. Rethinking the up-sampling operations in cnn-based generative network for generalizable deepfake detection. In *Proceedings of the IEEE/CVF Conference on Computer Vision and Pattern Recognition*, pages 28130–28139, 2024.
- [41] Aäron Van Den Oord, Nal Kalchbrenner, and Koray Kavukcuoglu. Pixel recurrent neural networks. In *International conference on machine learning*, pages 1747–1756. PMLR, 2016.
- [42] Sheng-Yu Wang et al. Cnn-generated images are surprisingly easy to spot... for now. In *Proceedings of the IEEE/CVF Conference on Computer Vision and Pattern Recognition*, pages 8695–8704, 2020.
- [43] SY Wang et al. Cnn-generated images are surprisingly easy to spot... for now. In *Proceedings of the IEEE/CVF Conference on Computer Vision and Pattern Recognition*, 2020.
- [44] Shitao Xiao, Yuezhe Wang, Junjie Zhou, Huaying Yuan, Xingrun Xing, Ruiran Yan, Chaofan Li, Shuting Wang, Tiejun Huang, and Zheng Liu. Omnigen: Unified image generation. *arXiv preprint arXiv:2409.11340*, 2024.
- [45] Zhipei Xu, Xuanyu Zhang, Runyi Li, Zecheng Tang, Qing Huang, and Jian Zhang. Fakeshield: Explainable image forgery detection and localization via multi-modal large language models. In *The Thirteenth International Conference on Learning Representations*, 2025.
- [46] Zhipei Xu, Xuanyu Zhang, Xing Zhou, and Jian Zhang. Avatarshield: Visual reinforcement learning for human-centric video forgery detection. *arXiv preprint arXiv:2505.15173*, 2025.
- [47] Jiazhen Yan, Fan Wang, Weiwei Jiang, Ziqiang Li, and Zhangjie Fu. Ns-net: Decoupling clip semantic information through null-space for generalizable ai-generated image detection. *arXiv preprint arXiv:2508.01248*, 2025.
- [48] Shilin Yan, Ouxiang Li, Jiayin Cai, Yanbin Hao, Xiaolong Jiang, Yao Hu, and Weidi Xie. A sanity check for ai-generated image detection. *arXiv preprint arXiv:2406.19435*, 2024.
- [49] Zhiyuan Yan, Kaiqing Lin, Zongjian Li, Junyan Ye, Hui Han, Zhendong Wang, Hao Liu, Bin Lin, Hao Li, Xue Xu, et al. Can understanding and generation truly benefit together—or just coexist? *arXiv preprint arXiv:2509.09666*, 2025.

- [50] Zhiyuan Yan, Jiangming Wang, Peng Jin, Ke-Yue Zhang, Chengchun Liu, Shen Chen, Taiping Yao, Shouhong Ding, Baoyuan Wu, and Li Yuan. Orthogonal subspace decomposition for generalizable ai-generated image detection. In *Forty-second International Conference on Machine Learning*.
- [51] Zhiyuan Yan, Taiping Yao, Shen Chen, Yandan Zhao, Xinghe Fu, Junwei Zhu, Donghao Luo, Chengjie Wang, Shouhong Ding, Yunsheng Wu, et al. Df40: Toward next-generation deepfake detection. *arXiv preprint arXiv:2406.13495*, 2024.
- [52] Zhiyuan Yan, Junyan Ye, Weijia Li, Zilong Huang, Shenghai Yuan, Xiangyang He, Kaiqing Lin, Jun He, Conghui He, and Li Yuan. Gpt-imgeval: A comprehensive benchmark for diagnosing gpt4o in image generation. *arXiv preprint arXiv:2504.02782*, 2025.
- [53] Xiao Yu, Kejiang Chen, Kai Zeng, Han Fang, Zijin Yang, Xiuwei Shang, Yuang Qi, Weiming Zhang, and Nenghai Yu. Semgir: Semantic-guided image regeneration based method for ai-generated image detection and attribution. In *Proceedings of the 32nd ACM International Conference on Multimedia*, pages 8480–8488, 2024.
- [54] Yabo Zhang, Yuxiang Wei, Dongsheng Jiang, Xiaopeng Zhang, Wangmeng Zuo, and Qi Tian. Controlvideo: Training-free controllable text-to-video generation. *arXiv preprint arXiv:2305.13077*, 2023.
- [55] Chende Zheng, Chenhao Lin, Zhengyu Zhao, Hang Wang, Xu Guo, Shuai Liu, and Chao Shen. Breaking semantic artifacts for generalized ai-generated image detection. *Advances in Neural Information Processing Systems*, 37:59570–59596, 2024.
- [56] Nan Zhong, Yiran Xu, Sheng Li, Zhenxing Qian, and Xinpeng Zhang. Patchcraft: Exploring texture patch for efficient ai-generated image detection. *arXiv preprint arXiv:2311.12397*, pages 1–18, 2024.
- [57] Yue Zhou, Bing Fan, Pradeep K. Atrey, and Feng Ding. Exposing deepfakes using dual-channel network with multi-axis attention and frequency analysis. In *Proceedings of the 2023 ACM Workshop on Information Hiding and Multimedia Security*, pages 169–174, 2023.
- [58] Yue Zhou, Xinan He, KaiQing Lin, Bin Fan, Feng Ding, and Bin Li. Breaking latent prior bias in detectors for generalizable aigc image detection. *arXiv preprint arXiv:2506.00874*, 2025.
- [59] Mingjian Zhu, Hanting Chen, Qiangyu Yan, Xudong Huang, Guanyu Lin, Wei Li, Zhijun Tu, Hailin Hu, Jie Hu, and Yunhe Wang. Genimage: A million-scale benchmark for detecting ai-generated image. *Advances in Neural Information Processing Systems*, 36:77771–77782, 2023.

The Appendix provides additional technical and evaluative details of our work. Section A presents the **implementation details** of DDA. Section B summarizes the **peer methods**. Section C **visualizes the degree of data alignment** of different methods in the feature space. Section D presents **ablation studies on input size and backbone**. Section E provides **details of our proposed dataset EvalGEN**, including example prompts used for generation and visualizations of selected samples. Finally, Section F **visualizes the regional detection results of DDA**.

## A Implementation Details

**Training Details.** All experiments were conducted on eight NVIDIA V100 GPUs. We trained the detector on a dataset consisting of MSCOCO images and their synthetic counterparts generated through DDA alignment using the VAE from Stable Diffusion 2.1. The model was optimized with a base batch size of 16 and a learning rate of  $1e-4$ . To achieve an effective batch size of 64 without exceeding GPU memory limits, gradient accumulation was applied over four iterations. Balanced accuracy was evaluated on all datasets every 10,000 iterations, and early stopping was employed to prevent overfitting. To help the model better shape its decision boundary, each batch was manually constructed to include both real images and their DDA-aligned counterparts, allowing the model to simultaneously observe closely aligned positive and negative samples.

## B Peer Methods

Below we provide a brief description of the compared methods used in Section 4 of main paper.

**NPR [8]** This detector leverages low-level features—neighboring pixel relationships—to distinguish synthetic images from real ones. NPR trains a ResNet-50 to identify upsampling patterns.

**UnivFD [32]** Instead of conventional supervised training, this method utilizes features from a vision-language model (CLIP-ViT) combined with a linear classifier. This approach avoids overfitting to specific generative artifacts and generalizes better to unseen generators.

**FatFormer [31]** FatFormer builds on a ViT backbone, incorporating a forgery-aware adapter that adapts features in both the image and frequency domains. It introduces language-guided alignment using contrastive learning with text prompts to improve generalization.

**SAFE [23]** This method focuses on frequency domain artifacts. The detector is built upon a ResNet backbone and trained with several data augmentation techniques, including random masking.

**C2P-CLIP [38]** The method utilizes CLIP embeddings with category-specific prompts to enhance deepfake detection generalizability. Image captions are generated using ClipCap and enhanced with category common prompts. During training, these enhanced caption-image pairs train the image encoder through contrastive learning. For inference, only the modified image encoder and a linear classifier are used.

**AIDE [48]** This work employs a hybrid approach that combines low-level patch statistics with high-level semantics. It uses DCT scoring to select extreme frequency patches for extracting noise patterns through SRM filters, while utilizing CLIP embeddings to capture semantic information. These complementary features are fused through channel-wise concatenation before classification.

**DRCT [4]** This method reconstructs real images using diffusion models to generate challenging synthetic samples that retain visual content while introducing subtle artifacts. Contrastive learning is employed to guide detectors toward recognizing these fingerprints, improving generalization.

**AlignedForensics [33]** This method creates aligned datasets by reconstructing real images through a single forward pass in an LDM’s autoencoder. This forces the detector to focus exclusively on artifacts introduced by the VAE decoder, avoiding reliance on spurious correlations.

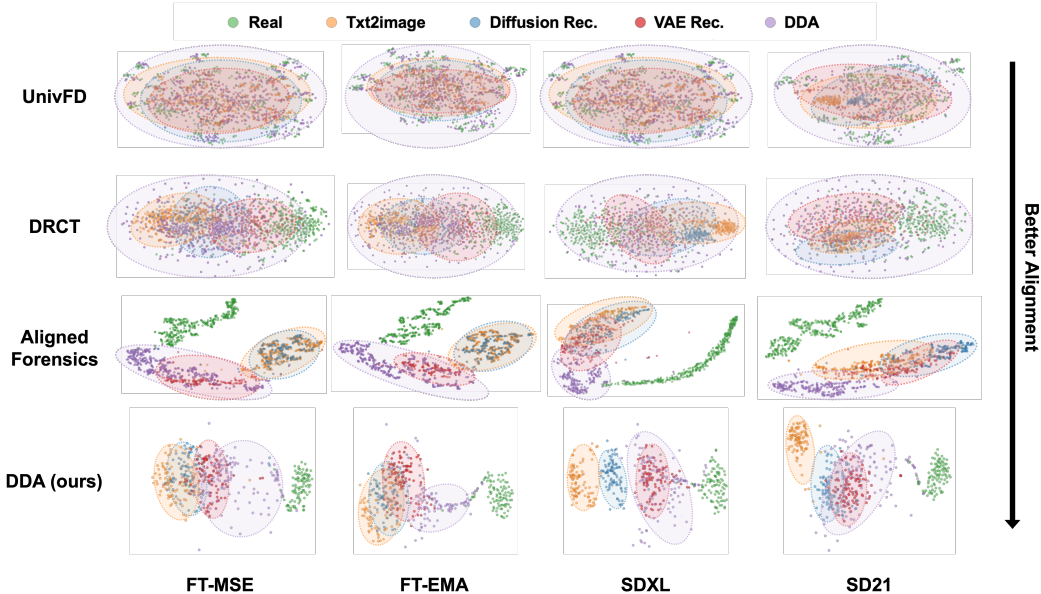


Figure 11: t-SNE visualizations comparing real and synthetic images using detectors trained with different data alignment methods. Rows correspond to the data alignment method used during detector training, while columns represent the generative pipeline—either VAE or diffusion—used to produce synthetic images. **The results show that detectors trained with better dataset alignment are able to separate reconstructed images more distinctly, highlighting the importance of effective dataset alignment in achieving clearer feature space separation.**

**B-Free [14]** B-Free introduces a training paradigm using self-conditioned diffusion-based reconstructions. It ensures semantic alignment between real and synthetic images so that differences arise solely from generation artifacts. The approach includes content augmentation via inpainting and fine-tunes a DINOv2+reg ViT using large crops to retain forensic signals.

## C More Comparison Results

**Comparison to Dataset Alignment Methods in Feature Domain** Fig 11 presents t-SNE visualizations of real and synthetic image features, generated by detectors trained with varying data alignment strategies. Each row, from top to bottom, represents detectors trained on datasets with progressively stronger alignment. **Detectors trained on better-aligned datasets yield more separable feature distributions, suggesting that enhanced alignment facilitates clearer decision boundaries between real and synthetic content.** These findings reinforce the role of data alignment in improving feature separability and overall AGI detector performance.

## D More Ablation Results

**Ablation on Input Size** Table 12 presents an ablation study of our method across different input sizes, ranging from 224 to 504. Detectors achieve comparable accuracies across these input sizes.

**Ablation on Backbone** Table 13 presents an ablation study comparing the performance of different backbone architectures. The ResNet backbone is excluded from this study due to training instability and failure to converge. The relatively poor performance of linear probing methods is attributed to the limited representational capacity of a single linear layer. This observation aligns with the convergence issues observed with ResNet, suggesting that the universal artifacts in our training data are inherently more difficult to learn. In contrast, AlignedForensics [33] successfully employs a ResNet backbone, implying that the artifacts used in our training setup may be subtler or more complex than those captured in prior work. Another key finding is that DINO-LoRA outperforms CLIP-LoRA. This

Table 12: Ablation study across different input sizes.

Input Size	GenImage	DRCT-2M	EvalGEN	Chameleon	SynthWildx	Avg
224	94.9	96.7	<b>97.2</b>	71.9	80.3	88.2 ± 11.5
252	<u>95.3</u>	96.7	94.1	72.0	84.0	88.4 ± 10.5
280	<b>95.7</b>	96.2	95.4	70.1	84.6	88.4 ± 11.3
392	92.9	96.5	95.7	71.8	89.6	<u>89.3</u> ± 10.2
448	93.4	<u>97.2</u>	89.5	65.7	<u>89.9</u>	87.1 ± 12.4
504	93.0	93.0	95.8	<u>73.2</u>	86.2	88.2 ± 9.1
<b>336</b>	91.7	<b>98.1</b>	96.3	<u>82.4</u>	<b>90.9</b>	<b>91.9</b> ± 6.1

Table 13: Ablation on backbones and training strategies. **Linear Probing** refers to training a linear classifier on frozen backbone features. **LoRA Finetune** denotes fine-tuning the backbone using LoRA (rank=8).

Train Strategy	Backbone	GenImage	DRCT-2M	EvalGEN	Chameleon	SynthWildx	Avg
Linear Probing	CLIP ViT-B/16	86.4	84.2	92.3	54.7	53.9	74.3 ± 18.5
	CLIP ViT-B/32	83.8	80.8	97.3	63.2	54.5	75.9 ± 17.1
	CLIP ViT-L/14	91.2	<u>91.2</u>	<u>98.9</u>	59.1	52.8	78.6 ± 21.1
	DINOv2 ViT-S/14	68.8	74.4	59.8	60.9	62.6	65.3 ± 6.2
	DINOv2 ViT-B/14	68.3	74.5	66.2	64.1	58.6	66.8 ± 4.9
	DINOv2 ViT-L/14	70.5	75.6	56.8	60.6	61.6	65.0 ± 7.8
LoRA Finetune	CLIP ViT-B/16	<u>95.2</u>	80.3	96.2	46.6	62.0	76.1 ± 21.5
	CLIP ViT-B/32	93.2	80.6	98.5	55.0	59.0	77.3 ± 19.7
	CLIP ViT-L/14	<b>97.0</b>	80.4	<b>99.2</b>	<u>67.7</u>	<u>71.8</u>	<u>83.2</u> ± 14.4
	<b>DINOv2 ViT-L/14</b>	91.7	<b>98.1</b>	96.3	<b>82.4</b>	<b>90.9</b>	<b>91.9</b> ± 6.1

performance difference is likely due to the architectural focus of each backbone: CLIP emphasizes high-level semantic features, while DINO is more attuned to low-level visual patterns—which are more indicative of AI-generated image artifacts. Moreover, DINO-LoRA achieves a lower standard deviation, indicating greater stability for robust AGI detection.

```

Prompt 00 a photo of a backpack
Prompt 01 a photo of a backpack below a cake
Prompt 02 a photo of a backpack right of a sandwich
Prompt 03 a photo of a banana
Prompt 04 a photo of a baseball bat
Prompt 05 a photo of a baseball bat and a bear
Prompt 06 a photo of a baseball bat and a fork
Prompt 07 a photo of a baseball bat and a giraffe
Prompt 08 a photo of a baseball glove
Prompt 09 a photo of a baseball glove and a carrot
Prompt 10 a photo of a baseball glove below an umbrella
Prompt 11 a photo of a baseball glove right of a bear
Prompt 12 a photo of a bear
Prompt 13 a photo of a bear above a clock
Prompt 14 a photo of a bear above a spoon
Prompt 15 a photo of a bed
Prompt 16 a photo of a bed right of a frisbee
Prompt 17 a photo of a bed right of a sports ball
Prompt 18 a photo of a bench
Prompt 19 a photo of a bench and a snowboard
...

```

## E More Details of EvalGEN

To construct EvalGEN, we used 553 distinct prompts, each generating 20 synthetic images per generator, resulting in 11,060 images per generator and a total of 55,300 synthetic images in the complete dataset. All images are stored in JPEG format with a quality factor of 96. A subset of prompts is provided above to illustrate the dataset’s diversity and semantic coverage, while

Fig. 12 shows visual examples from EvalGEN. To balance efficiency and representativeness, for the comparison in Table 2 and Table 10 of the main paper, we selected the first (index 0) image generated for each prompt, yielding  $55,300 / 20 = 2,765$  samples for quantitative evaluation.

## **F Regional Detection Analysis**

Figure 13 displays heatmaps of detection scores across segmented image regions, with numerical overlays indicating the detector’s predictions. These results reveal that detection scores vary by region, indicating that synthetic artifacts are spatially uneven. This observation suggests that localized detection strategies could further enhance robustness.

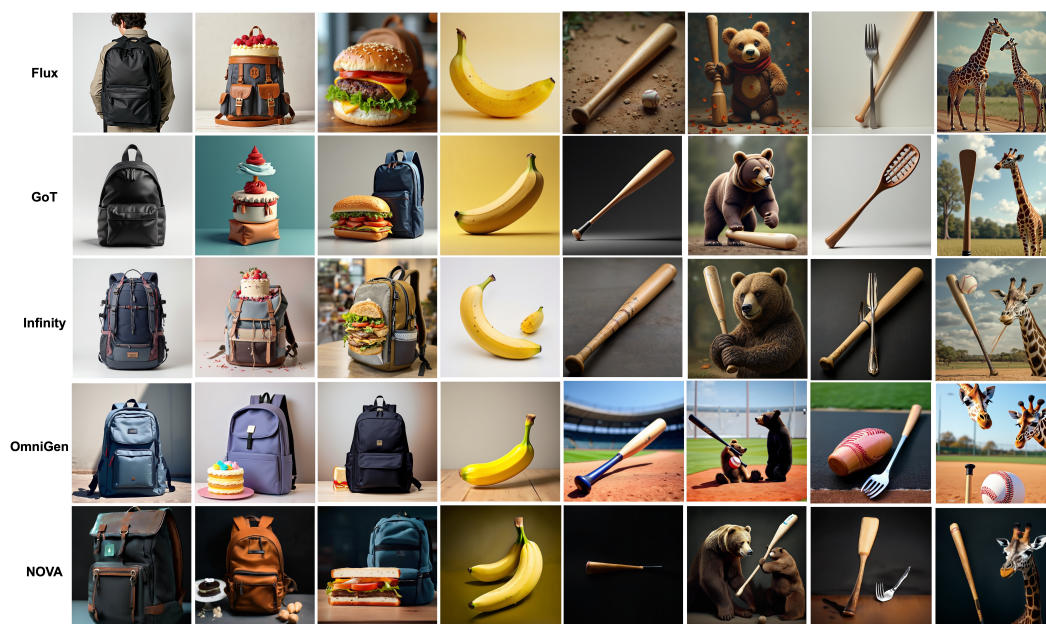


Figure 12: Examples from EvalGEN.



Figure 13: Patch-level detection results. From top to bottom, images are sourced from Synthbuster [1], Chameleon [48], ForenSynths [43], SynthWildx [7], AIGCDetectionBenchmark [56], WildRF [2], and EvalGEN (ours), respectively.

## NeurIPS Paper Checklist

### 1. Claims

Question: Do the main claims made in the abstract and introduction accurately reflect the paper's contributions and scope?

Answer: [Yes]

Justification: Refer to Abstract and Section 1

Guidelines:

- The answer NA means that the abstract and introduction do not include the claims made in the paper.
- The abstract and/or introduction should clearly state the claims made, including the contributions made in the paper and important assumptions and limitations. A No or NA answer to this question will not be perceived well by the reviewers.
- The claims made should match theoretical and experimental results, and reflect how much the results can be expected to generalize to other settings.
- It is fine to include aspirational goals as motivation as long as it is clear that these goals are not attained by the paper.

### 2. Limitations

Question: Does the paper discuss the limitations of the work performed by the authors?

Answer: [Yes]

Justification: Refer to Section 5

Guidelines:

- The answer NA means that the paper has no limitation while the answer No means that the paper has limitations, but those are not discussed in the paper.
- The authors are encouraged to create a separate "Limitations" section in their paper.
- The paper should point out any strong assumptions and how robust the results are to violations of these assumptions (e.g., independence assumptions, noiseless settings, model well-specification, asymptotic approximations only holding locally). The authors should reflect on how these assumptions might be violated in practice and what the implications would be.
- The authors should reflect on the scope of the claims made, e.g., if the approach was only tested on a few datasets or with a few runs. In general, empirical results often depend on implicit assumptions, which should be articulated.
- The authors should reflect on the factors that influence the performance of the approach. For example, a facial recognition algorithm may perform poorly when image resolution is low or images are taken in low lighting. Or a speech-to-text system might not be used reliably to provide closed captions for online lectures because it fails to handle technical jargon.
- The authors should discuss the computational efficiency of the proposed algorithms and how they scale with dataset size.
- If applicable, the authors should discuss possible limitations of their approach to address problems of privacy and fairness.
- While the authors might fear that complete honesty about limitations might be used by reviewers as grounds for rejection, a worse outcome might be that reviewers discover limitations that aren't acknowledged in the paper. The authors should use their best judgment and recognize that individual actions in favor of transparency play an important role in developing norms that preserve the integrity of the community. Reviewers will be specifically instructed to not penalize honesty concerning limitations.

### 3. Theory assumptions and proofs

Question: For each theoretical result, does the paper provide the full set of assumptions and a complete (and correct) proof?

Answer: [Yes]

Justification: Refer to Section 3.2

Guidelines:

- The answer NA means that the paper does not include theoretical results.
- All the theorems, formulas, and proofs in the paper should be numbered and cross-referenced.
- All assumptions should be clearly stated or referenced in the statement of any theorems.
- The proofs can either appear in the main paper or the supplemental material, but if they appear in the supplemental material, the authors are encouraged to provide a short proof sketch to provide intuition.
- Inversely, any informal proof provided in the core of the paper should be complemented by formal proofs provided in appendix or supplemental material.
- Theorems and Lemmas that the proof relies upon should be properly referenced.

#### 4. Experimental result reproducibility

Question: Does the paper fully disclose all the information needed to reproduce the main experimental results of the paper to the extent that it affects the main claims and/or conclusions of the paper (regardless of whether the code and data are provided or not)?

Answer: [Yes]

Justification: Refer to Section 4

Guidelines:

- The answer NA means that the paper does not include experiments.
- If the paper includes experiments, a No answer to this question will not be perceived well by the reviewers: Making the paper reproducible is important, regardless of whether the code and data are provided or not.
- If the contribution is a dataset and/or model, the authors should describe the steps taken to make their results reproducible or verifiable.
- Depending on the contribution, reproducibility can be accomplished in various ways. For example, if the contribution is a novel architecture, describing the architecture fully might suffice, or if the contribution is a specific model and empirical evaluation, it may be necessary to either make it possible for others to replicate the model with the same dataset, or provide access to the model. In general, releasing code and data is often one good way to accomplish this, but reproducibility can also be provided via detailed instructions for how to replicate the results, access to a hosted model (e.g., in the case of a large language model), releasing of a model checkpoint, or other means that are appropriate to the research performed.
- While NeurIPS does not require releasing code, the conference does require all submissions to provide some reasonable avenue for reproducibility, which may depend on the nature of the contribution. For example
  - (a) If the contribution is primarily a new algorithm, the paper should make it clear how to reproduce that algorithm.
  - (b) If the contribution is primarily a new model architecture, the paper should describe the architecture clearly and fully.
  - (c) If the contribution is a new model (e.g., a large language model), then there should either be a way to access this model for reproducing the results or a way to reproduce the model (e.g., with an open-source dataset or instructions for how to construct the dataset).
  - (d) We recognize that reproducibility may be tricky in some cases, in which case authors are welcome to describe the particular way they provide for reproducibility. In the case of closed-source models, it may be that access to the model is limited in some way (e.g., to registered users), but it should be possible for other researchers to have some path to reproducing or verifying the results.

#### 5. Open access to data and code

Question: Does the paper provide open access to the data and code, with sufficient instructions to faithfully reproduce the main experimental results, as described in supplemental material?

Answer: [Yes]

Justification: Refer to Abstract

Guidelines:

- The answer NA means that paper does not include experiments requiring code.
- Please see the NeurIPS code and data submission guidelines (<https://nips.cc/public/guides/CodeSubmissionPolicy>) for more details.
- While we encourage the release of code and data, we understand that this might not be possible, so “No” is an acceptable answer. Papers cannot be rejected simply for not including code, unless this is central to the contribution (e.g., for a new open-source benchmark).
- The instructions should contain the exact command and environment needed to run to reproduce the results. See the NeurIPS code and data submission guidelines (<https://nips.cc/public/guides/CodeSubmissionPolicy>) for more details.
- The authors should provide instructions on data access and preparation, including how to access the raw data, preprocessed data, intermediate data, and generated data, etc.
- The authors should provide scripts to reproduce all experimental results for the new proposed method and baselines. If only a subset of experiments are reproducible, they should state which ones are omitted from the script and why.
- At submission time, to preserve anonymity, the authors should release anonymized versions (if applicable).
- Providing as much information as possible in supplemental material (appended to the paper) is recommended, but including URLs to data and code is permitted.

## 6. Experimental setting/details

Question: Does the paper specify all the training and test details (e.g., data splits, hyper-parameters, how they were chosen, type of optimizer, etc.) necessary to understand the results?

Answer: [Yes]

Justification: Refer to Section 4

Guidelines:

- The answer NA means that the paper does not include experiments.
- The experimental setting should be presented in the core of the paper to a level of detail that is necessary to appreciate the results and make sense of them.
- The full details can be provided either with the code, in appendix, or as supplemental material.

## 7. Experiment statistical significance

Question: Does the paper report error bars suitably and correctly defined or other appropriate information about the statistical significance of the experiments?

Answer: [Yes]

Justification: Refer to Section 4

Guidelines:

- The answer NA means that the paper does not include experiments.
- The authors should answer "Yes" if the results are accompanied by error bars, confidence intervals, or statistical significance tests, at least for the experiments that support the main claims of the paper.
- The factors of variability that the error bars are capturing should be clearly stated (for example, train/test split, initialization, random drawing of some parameter, or overall run with given experimental conditions).
- The method for calculating the error bars should be explained (closed form formula, call to a library function, bootstrap, etc.)
- The assumptions made should be given (e.g., Normally distributed errors).
- It should be clear whether the error bar is the standard deviation or the standard error of the mean.

- It is OK to report 1-sigma error bars, but one should state it. The authors should preferably report a 2-sigma error bar than state that they have a 96% CI, if the hypothesis of Normality of errors is not verified.
- For asymmetric distributions, the authors should be careful not to show in tables or figures symmetric error bars that would yield results that are out of range (e.g. negative error rates).
- If error bars are reported in tables or plots, The authors should explain in the text how they were calculated and reference the corresponding figures or tables in the text.

#### 8. Experiments compute resources

Question: For each experiment, does the paper provide sufficient information on the computer resources (type of compute workers, memory, time of execution) needed to reproduce the experiments?

Answer: [Yes]

Justification: Refer to Section 4

Guidelines:

- The answer NA means that the paper does not include experiments.
- The paper should indicate the type of compute workers CPU or GPU, internal cluster, or cloud provider, including relevant memory and storage.
- The paper should provide the amount of compute required for each of the individual experimental runs as well as estimate the total compute.
- The paper should disclose whether the full research project required more compute than the experiments reported in the paper (e.g., preliminary or failed experiments that didn't make it into the paper).

#### 9. Code of ethics

Question: Does the research conducted in the paper conform, in every respect, with the NeurIPS Code of Ethics <https://neurips.cc/public/EthicsGuidelines?>

Answer: [Yes]

Justification: Research conducted in this paper conform with the NeurIPS Code of Ethics in every respect

Guidelines:

- The answer NA means that the authors have not reviewed the NeurIPS Code of Ethics.
- If the authors answer No, they should explain the special circumstances that require a deviation from the Code of Ethics.
- The authors should make sure to preserve anonymity (e.g., if there is a special consideration due to laws or regulations in their jurisdiction).

#### 10. Broader impacts

Question: Does the paper discuss both potential positive societal impacts and negative societal impacts of the work performed?

Answer: [Yes]

Justification: Refer to Section 5

Guidelines:

- The answer NA means that there is no societal impact of the work performed.
- If the authors answer NA or No, they should explain why their work has no societal impact or why the paper does not address societal impact.
- Examples of negative societal impacts include potential malicious or unintended uses (e.g., disinformation, generating fake profiles, surveillance), fairness considerations (e.g., deployment of technologies that could make decisions that unfairly impact specific groups), privacy considerations, and security considerations.

- The conference expects that many papers will be foundational research and not tied to particular applications, let alone deployments. However, if there is a direct path to any negative applications, the authors should point it out. For example, it is legitimate to point out that an improvement in the quality of generative models could be used to generate deepfakes for disinformation. On the other hand, it is not needed to point out that a generic algorithm for optimizing neural networks could enable people to train models that generate Deepfakes faster.
- The authors should consider possible harms that could arise when the technology is being used as intended and functioning correctly, harms that could arise when the technology is being used as intended but gives incorrect results, and harms following from (intentional or unintentional) misuse of the technology.
- If there are negative societal impacts, the authors could also discuss possible mitigation strategies (e.g., gated release of models, providing defenses in addition to attacks, mechanisms for monitoring misuse, mechanisms to monitor how a system learns from feedback over time, improving the efficiency and accessibility of ML).

## 11. Safeguards

Question: Does the paper describe safeguards that have been put in place for responsible release of data or models that have a high risk for misuse (e.g., pretrained language models, image generators, or scraped datasets)?

Answer: [NA]

Justification: The paper poses no risk for misuse

Guidelines:

- The answer NA means that the paper poses no such risks.
- Released models that have a high risk for misuse or dual-use should be released with necessary safeguards to allow for controlled use of the model, for example by requiring that users adhere to usage guidelines or restrictions to access the model or implementing safety filters.
- Datasets that have been scraped from the Internet could pose safety risks. The authors should describe how they avoided releasing unsafe images.
- We recognize that providing effective safeguards is challenging, and many papers do not require this, but we encourage authors to take this into account and make a best faith effort.

## 12. Licenses for existing assets

Question: Are the creators or original owners of assets (e.g., code, data, models), used in the paper, properly credited and are the license and terms of use explicitly mentioned and properly respected?

Answer: [Yes]

Justification: Refer to Section 4

Guidelines:

- The answer NA means that the paper does not use existing assets.
- The authors should cite the original paper that produced the code package or dataset.
- The authors should state which version of the asset is used and, if possible, include a URL.
- The name of the license (e.g., CC-BY 4.0) should be included for each asset.
- For scraped data from a particular source (e.g., website), the copyright and terms of service of that source should be provided.
- If assets are released, the license, copyright information, and terms of use in the package should be provided. For popular datasets, [paperswithcode.com/datasets](https://paperswithcode.com/datasets) has curated licenses for some datasets. Their licensing guide can help determine the license of a dataset.
- For existing datasets that are re-packaged, both the original license and the license of the derived asset (if it has changed) should be provided.

- If this information is not available online, the authors are encouraged to reach out to the asset’s creators.

### 13. **New assets**

Question: Are new assets introduced in the paper well documented and is the documentation provided alongside the assets?

Answer: [Yes]

Justification: Refer to Supplementary

Guidelines:

- The answer NA means that the paper does not release new assets.
- Researchers should communicate the details of the dataset/code/model as part of their submissions via structured templates. This includes details about training, license, limitations, etc.
- The paper should discuss whether and how consent was obtained from people whose asset is used.
- At submission time, remember to anonymize your assets (if applicable). You can either create an anonymized URL or include an anonymized zip file.

### 14. **Crowdsourcing and research with human subjects**

Question: For crowdsourcing experiments and research with human subjects, does the paper include the full text of instructions given to participants and screenshots, if applicable, as well as details about compensation (if any)?

Answer: [NA]

Justification: The paper does not involve crowdsourcing nor research with human subjects

Guidelines:

- The answer NA means that the paper does not involve crowdsourcing nor research with human subjects.
- Including this information in the supplemental material is fine, but if the main contribution of the paper involves human subjects, then as much detail as possible should be included in the main paper.
- According to the NeurIPS Code of Ethics, workers involved in data collection, curation, or other labor should be paid at least the minimum wage in the country of the data collector.

### 15. **Institutional review board (IRB) approvals or equivalent for research with human subjects**

Question: Does the paper describe potential risks incurred by study participants, whether such risks were disclosed to the subjects, and whether Institutional Review Board (IRB) approvals (or an equivalent approval/review based on the requirements of your country or institution) were obtained?

Answer: [NA]

Justification: The paper does not involve crowdsourcing nor research with human subjects

Guidelines:

- The answer NA means that the paper does not involve crowdsourcing nor research with human subjects.
- Depending on the country in which research is conducted, IRB approval (or equivalent) may be required for any human subjects research. If you obtained IRB approval, you should clearly state this in the paper.
- We recognize that the procedures for this may vary significantly between institutions and locations, and we expect authors to adhere to the NeurIPS Code of Ethics and the guidelines for their institution.
- For initial submissions, do not include any information that would break anonymity (if applicable), such as the institution conducting the review.

### 16. **Declaration of LLM usage**

Question: Does the paper describe the usage of LLMs if it is an important, original, or non-standard component of the core methods in this research? Note that if the LLM is used only for writing, editing, or formatting purposes and does not impact the core methodology, scientific rigorousness, or originality of the research, declaration is not required.

Answer: [NA]

Justification: Refer to Section 3.2

Guidelines:

- The answer NA means that the core method development in this research does not involve LLMs as any important, original, or non-standard components.
- Please refer to our LLM policy (<https://neurips.cc/Conferences/2025/LLM>) for what should or should not be described.